

Hot spin spots in the laser-induced demagnetization

M. S. Si

*Department of Physics, Indiana State University, Terre Haute, Indiana 47809, &
Key Laboratory for Magnetism and Magnetic Materials of the Ministry of Education,
Lanzhou University, Lanzhou 730000, China*

G. P. Zhang*

¹*Department of Physics, Indiana State University, Terre Haute, Indiana 47809*

(Dated: February 21, 2012)

Abstract

Laser-induced femtosecond magnetism or femtomagnetism simultaneously relies on two distinctive contributions: (a) the optical dipole interaction (ODI) between a laser field and a magnetic system and (b) the spin expectation value change (SEC) between two transition states. Surprisingly, up to now, no study has taken both contributions into account simultaneously. Here we do so by introducing a new concept of the optical spin generator, a product of SEC and ODI between transition states. In ferromagnetic nickel, our first-principles calculation demonstrates that the larger the value of optical spin generator is, the larger the dynamic spin moment change is. This simple generator directly links the time-dependent spin moment change $\Delta M_z^{\mathbf{k}}(t)$ at every crystal-momentum \mathbf{k} point to its intrinsic electronic structure and magnetic properties. Those hot spin spots are a direct manifestation of the optical spin generator, and should be the focus of future research.

PACS numbers: 75.40.Gb, 78.20.Ls, 75.70.-i, 78.47.J-

Keywords:

Femtomagnetism represents an emerging frontier in magnetic recording technology [1, 2], where a femtosecond laser pulse is used to read/write the magnetic information in the storage media within a few hundred femtoseconds. However, how such an ultrafast magnetization process occurs is not well understood. The true underlying microscopic mechanism is still under debate. Two major mechanisms are proposed. One is the Elliot-Yafet (EY) mechanism proposed by Koopmans *et al.* [3, 4], in which the spin relaxation occurs via electron scattering at impurities or defects and phonons. Further, Steiauf *et al.* [5] invoked a strong spin-mixing parameter to support the EY mechanism. However, the EY mechanism is challenged in rare earth compounds as Vahaplar *et al.* [6] demonstrated a nonthermal writing on a time scale of 10 ps. On such a long time scale, the phonon should play an important role by smearing out any initial polarization dependence on the laser light. In a group of the lanthanide-doped permalloys, Radu *et al.* [7] particularly reported an opposite behavior to the EY's prediction [3]. Nonthermal nature of femtomagnetism was clearly demonstrated in GdFeCo [8], which also invalidated stimulated Raman scattering mechanism. Another mechanism attributes the demagnetization to the coherent interaction of the laser beam with the electron of the system proposed by Bigot *et al.* [9]. In systems with spin-orbit coupling in general most of the optical electric dipole transitions of the stimulated electrons conserve the dominant spin character of the electrons, but a few transitions are spin-flip transitions. The number of spin-flip transitions increases with increasing spin-orbit coupling. The coherent interaction mechanism is strongly supported by the theoretical findings independently developed by Zhang *et al.* [10, 11], and they found that a crucial cooperation between laser field and spin-orbit coupling is indispensable to ultrafast demagnetization. In 2009, Lefkidis *et al.* [12] proposed a spin-switch mechanism in the coherent temporal regime, which is based on the angular-momentum exchange between the light and the irradiated antiferromagnets. Motivated by those latest investigations, here we provide a new view on the coherent interaction mechanism in femtosecond magnetism.

To this end, the existing experimental results are not conclusive enough to develop a simple method to characterize the spin moment change in femtomagnetism. In particular, little attention has been paid to two most important contributions simultaneously: *Optical dipole interaction* (ODI) and *spin expectation value change* (SEC). SEC is defined as the difference between the spin expectation values of two transition states. ODI allows the laser pulse to influence the system, while SEC allows the spin moment change during laser

excitation. However, those two contributions are intrinsically disconnected. For instance, the dipole interaction does not guarantee spin moment change. In optical dipole transitions, without spin-orbit coupling, the spin is conserved. The separation of ODI and SEC is unique to femtomagnetism, and is very different from the magnetization process driven by a thermal or magnetic field, where the spin moment change is the only quantity that should be considered. Therefore, to fully understand femtomagnetism, it is a must to take both contributions into account simultaneously.

In this Letter we take into account both contributions by introducing a new concept - optical spin generator or \mathcal{SD} . This generator is defined as a product of optical dipole transition moment and SEC for a particular transition. If multiple transitions are involved, a summation over those transitions should be carried out. We test this concept in ferromagnetic nickel. Our first-principles calculation shows that \mathcal{SD} has the capability to single out optically hot spin spots. In nickel, two major hot spots are identified. Their structures in the Brillouin zone are almost identical to those constructed from the optical spin generator. Therefore, our finding not only greatly simplifies the interpretation of femtomagnetism, but also points out a new direction for future experimental investigations.

We start with a transition from state $|a\rangle$ to state $|b\rangle$. The expectation value of optical spin generator \mathcal{SD} is defined as

$$(\mathcal{SD})_{ab} \equiv D_{a \rightarrow b} \Delta S_{a \rightarrow b} + c.c. \quad (1)$$

where $D_{a \rightarrow b}$ is a dipole transition moment, $\Delta S_{a \rightarrow b} = S_b - S_a$ is SEC and S_a refers to the spin expectation value in state $|a\rangle$, and $c.c.$ refers to the complex conjugation. The direction indices of \mathcal{SD} are omitted for brevity. To see an analytic example, we resort to two states characterized by total angular momentum quantum number j and its magnetic quantum number m_j . First, we form the eigenstates for each j and m_j . Then, we compute the dipole transition matrix element and the spin matrix element among those states. Finally, we compute the product of these two matrix elements. A lengthy but straightforward calculation [13] shows that for a transition with $\Delta m_j = 0$ and $\Delta j = 1$, the expectation value of $(\mathcal{SD})_{ab}$ generator for this transition is

$$(\mathcal{SD})_{ab} = -\frac{1}{2} \sqrt{\left(1 - \frac{m_j^2}{(j+1)^2}\right) \left(\frac{m_j}{j(j+1)}\right)^2}, \quad (2)$$

where the radial contribution and its unit are not included. One sees explicitly that the

expectation value of optical spin generator nonlinearly depends on j and m_j ; such a nonlinear dependence results from their distinct dependence of spin and dipole expectation values on j and m_j though both spin and dipole changes monotonically with j and m_j , a finding which is verified in an entirely different system [14].

In the following, we are going to demonstrate the power of optical spin generator \mathcal{SD} in ferromagnetic nickel. While the details of our theoretical formalism have been presented before [11], here in brief, we start our calculation by solving the Kohn-Sham equation self-consistently. The spin-orbit coupling (SOC) is included explicitly, without using a spin mixing parameter [15]. Once we obtain eigenstates $(\psi_{n\mathbf{k}}, \mathcal{E}_{n\mathbf{k}})$, we then compute the spin and optical properties. We find that to converge our spin change, the number of required \mathbf{k} -points exceeds 87^3 (104^3 used in this study) in the Brillouin zone, which immediately imposes a big challenge for all the latter calculations. To test the accuracy of our results, Figures 1(a) and (b) show the Fermi surfaces on two high symmetry planes, where the agreement with the previous calculations [16, 17] is excellent. Note that there are two subbands - one for each dominant spin orientation - though they are mixed up due to SOC.

The interaction between the fs laser pulse field and the system is described by $H_I = -\mathbf{D} \cdot \mathbf{E}(t)$. Here $\mathbf{D} = e\mathbf{r}$ is the electric-dipole operator with e being the electron charge and \mathbf{r} the position operator. The dipole matrix elements are directly computed from the first-principles method, without using the constant matrix element approximation as others [15], which has a serious consequence (see below). The laser field $\mathbf{E}(t)$ peaks at 0 fs and has a Gaussian shape with duration of 12 fs and photon energy of 2 eV. We numerically solve the Liouville equation for the electron density matrices $\rho_{\mathbf{k}}$ at each \mathbf{k} point [18],

$$i\hbar \frac{\partial \rho_{\mathbf{k}}}{\partial t} = [H, \rho_{\mathbf{k}}], \quad (3)$$

where $H = H_0 + H_I$. Due to the huge number of \mathbf{k} points, all the calculations are run in parallel [18]. The spin moment change at each \mathbf{k} point is computed from $\Delta M_z^{\mathbf{k}}(t) = M_z^{\mathbf{k}}(t) - M_z^{\mathbf{k}}(-\infty)$, where the spin moment at \mathbf{k} point is $M_z^{\mathbf{k}}(t) = \text{Tr}[\rho_{\mathbf{k}} S_{\mathbf{k}}^z]$, and $S_{\mathbf{k}}^z$ is the z -component of spin matrix. Since the spin moment change oscillates with time, we time-average it from 90 to 150 fs; averaging the changes from 120 to 150 fs yields a similar result.

We first show that those conventional high symmetry lines and planes in the Brillouin zone are not a good guide for spin moment change. Figures 1(a)-(c) show the crystal-momentum-

resolved major magnetic spin moment changes $\Delta M_z^{\mathbf{k}}(t)$ on those traditional high symmetry lines and planes, where the filled circles denote the moment increase and the empty circles the moment reduction, with quantitative changes shown below each figure. In the Γ -X-W-K plane, the major spin reductions occur close to the Fermi surface (see Fig. 1(a)), but in the Γ -K-L-U-X plane, the major change is away from the Fermi surface. The maximum reduction reaches $-0.22\mu_B$. The hexagonal L-K-W-U-W' plane, which does not intersect with the Fermi surface, has a major change around the L-U line. Note that k points with the spin moment increase also appear in these planes. The net spin change comes from the superposition of the two types hot spots.

Next we demonstrate the power of optical spin generator to characterize the spin moment change in two steps: (1) we thoroughly examine the spin moment change $\Delta M_z^{\mathbf{k}}(t)$ at each \mathbf{k} in the entire Brillouin zone and (2) directly compute the \mathcal{SD} and compare it with the real spin moment change. Figure 2(a) illustrates the first comprehensive dispersion of $\Delta M_z^{\mathbf{k}}(t)$, which is constructed out of 73763 irreducible k points. To reduce the huge volume of the data, we only plot 750 k points with spin moment change $\Delta M_z^{\mathbf{k}}$ smaller than $-0.1\mu_B$ (more negative). This comprehensive dispersion finally narrows our attention to only two major spin hot spots and some small islands. Our findings are insightful. First, structurally the hot spin spots consist of stacks of layers of spin hot points in the crystal momentum space. These hot spots with large spin moment reduction are big enough to be detected experimentally. A small portion of spot B is displayed at the bottom left of the figure, with one representative layer magnified on the bottom right. Then we choose a triangle, highlighted by dark red balls, for a close examination. Choosing such a triangle is purely arbitrary, and is mainly in the consideration of the continuation of the coordinates of the \mathbf{k} -points; the conclusion is same when we choose a different triangle in different layers. To define the above triangle, we choose three \mathbf{k} -points, \mathbf{k}_1 , \mathbf{k}_2 , and \mathbf{k}_3 , whose coordinates are given in the caption of Fig. 2.

Second, different from the single-channel excitation process as seen in our above analytic example, the laser photon pre-selects multiple channels. To see this clearly, we present the energy band dispersion along three sides of the triangle (see Figure 2(d)). There are two transitions with their transition energies close to the laser photon energy, see two vertical arrows. According to our previous investigation [19], this leads to a possible resonant excitation. Therefore, the generator is constructed by summing over all the major transitions

as $(\mathcal{SD})_{\mathbf{k}} \equiv \sum_{ij} \Delta S_{\mathbf{k};ij}^z D_{\mathbf{k};ij}$, with i and j being the initial and final state band indices. In our present case, there are two such transitions. The results are illustrated in Fig. 2(b). The hot spin spots are nicely reproduced by \mathcal{SD} except the small islands. This explicitly shows that the \mathcal{SD} is able to characterize the spin moment change of femtomagnetism in the crystal-momentum space. Figure 2(e) compares the dispersion of spin moment change with that of \mathcal{SD} . We see that from \mathbf{k}_1 to \mathbf{k}_2 , \mathcal{SD} drops initially (more negative) and then increases sharply (less negative) when close to \mathbf{k}_2 . These changes are a joint effect of the SEC and dipole moment. As seen in the above analytic example, the change is highly nonlinear. This is partly due to the fact that ΔS and D generally depend on quantum numbers and \mathbf{k} points differently. Going from \mathbf{k}_2 to \mathbf{k}_3 , we see a monotonous decrease (more negative). On the \mathbf{k}_3 - \mathbf{k}_1 side, \mathcal{SD} shows a peak. These changes will manifest themselves in the spin moment change at each \mathbf{k} point.

Figure 2(e) shows the spin moment change $\Delta M_z^{\mathbf{k}}$ along three sides of the same triangle. It is astonishing that $\Delta M_z^{\mathbf{k}}$ closely follows \mathcal{SD} , with all main features reproduced. The difference is that \mathcal{SD} is computed solely from the SEC and dipole matrix elements while $\Delta M_z^{\mathbf{k}}$ is computed dynamically. Our additional extensive calculations (not included in the paper) yield the same conclusion. This proves unambiguously that \mathcal{SD} largely governs the nature of laser-induced spin dynamics. If we compare those two figures more closely, we do see some differences between $\Delta M_z^{\mathbf{k}}$ and \mathcal{SD} . For instance, along the \mathbf{k}_1 - \mathbf{k}_2 side, \mathcal{SD} has a smaller decrease than that in $\Delta M_z^{\mathbf{k}}$; along the \mathbf{k}_2 - \mathbf{k}_3 side there is a kink in $\Delta M_z^{\mathbf{k}}$. Along the \mathbf{k}_3 - \mathbf{k}_1 side, the spin moment change is also much more pronounced than that in \mathcal{SD} . These small differences are directly associated with the laser pulse shape and the photon energy. Notwithstanding these small difference, the optical spin generator provides an easy way to evaluate the spin moment change, without complicated real time simulations.

Conceptually, the optical spin generator is very useful for future experimental and theoretical investigations, not only in ferromagnets but also in magnetic semiconductors, since \mathcal{SD} is essentially a system quantity, and the only external input to construct \mathcal{SD} is the energy window set by laser photon energy. The physics meaning of \mathcal{SD} is very clear: It acts as a source term for the laser to influence spin. We emphasize that had we used the constant dipole matrix, \mathcal{SD} would be a simple spin matrix, and the optical dipole selection rule would be ignored. The hot spin spots are a manifestation of \mathcal{SD} . Future experimental research should be able to test our results.

In conclusion, we have introduced a new concept of the optical spin generator to simultaneously take into account both the dipole transition and spin expectation value change between transition states, each of which is indispensable to laser-induced femtosecond magnetism. The generator directly links to the spin moment change at each \mathbf{k} point. This helps to unfold the hidden kernel of femtomagnetism in crystal-momentum space. In ferromagnetic nickel, we find that the hot spin spots consist of two major spin hot spots and a few smaller islands. These hot spots are not along any high symmetry lines or plane nor Fermi surfaces. Instead they are determined by \mathcal{SD} . Within these hot spots, the \mathbf{k} -dispersed spin moment changes closely follow those of \mathcal{SD} and the effect of the laser pulse is reflected from the spectral transition window pre-selected by the photon energy. This provides a simple method to characterize the magnetization change on femtosecond time scale. Future experiments can directly test our prediction by focusing spin changes at those crystal momenta.

This work was supported by the U. S. Department of Energy under Contract No. DE-FG02-06ER46304. This work was also supported by the National Science Foundation of China (NSFC) under No. 10804038, and the Fundamental Research Fund for the Central Universities and Physics and Mathematics of Lanzhou University. We acknowledge part of the work as done on Indiana State University's high-performance computers. This research used resources of the National Energy Research Scientific Computing Center at Lawrence Berkeley National Laboratory, which is supported by the Office of Science of the U.S. Department of Energy under Contract No. DE-AC02-05CH11231. Our calculation also used resources of the Argonne Leadership Computing Facility at Argonne National Laboratory, which is supported by the Office of Science of the U. S. Department of Energy under Contract No. DE-AC02-06CH11357.

*Communication should be directed to GPZ. Email: gpzhang@indstate.edu

-
- [1] C. Boeglin, E. Beaupaire, V. Halte, V. Lopez-Flores, C. Stamm, N. Pontius, H. A. Dürr, and J.-Y. Bigot, *Nature* **465**, 458 (2010); A. Kirilyuk, A. V. Kimel, and Th. Rasing, *Rev. Mod. Phys.* **82**, 2731 (2010).
 - [2] E. Beaupaire, J.-C. Merle, A. Daunois, and J.-Y. Bigot, *Phys. Rev. Lett.* **76**, 4250 (1996).
 - [3] B. Koopmans, J. J. M. Ruigrok, F. Dalla Longa, and W. J. M. de Jonge *Phys. Rev. Lett.* **95**,

267207 (2005).

- [4] B. Koopmans, G. Malinowski, F. Dalla Longa, D. Steiauf, M. Föhnle, T. Roth, M. Cinchetti, M. Aeschlimann, *Nature Mater.* **9**, 259 (2010); M. G. Münzenberg, **9**, 184 (2010).
- [5] D. Steiauf and M. Föhnle, *Phys. Rev. B* **79**, 140401(R) (2009).
- [6] K. Vahaplar, A. M. Kalashnikova, A. V. Kimel, D. Hinzke, U. Nowak, R. Chantrell, A. Tsukamoto, A. Itoh, A. Kirilyuk, and Th. Rasing, *Phys. Rev. Lett.* **103**, 117201 (2009).
- [7] I. Radu, G. Woltersdorf, M. Kiessling, A. Melnikov, U. Bovensiepen, J.-U. Thiele, and C. H. Back, *Phys. Rev. Lett.* **102**, 117201 (2009).
- [8] J. Hohlfeld, C. D. Stanciu, and A. Rebei, *Appl. Phys. Lett.* **94**, 152504 (2009).
- [9] J.-Y. Bigot, M. Vomir, and E. Beaurepaire, *Nature Phys.* **5**, 515 (2009).
- [10] G. P. Zhang and W. Hübner, *Phys. Rev. Lett.* **85**, 3025 (2000).
- [11] G. P. Zhang, W. Hübner, G. Lefkidis, Y. H. Bai, and T. F. George, *Nature Phys.* **5**, 499 (2009).
- [12] G. Lefkidis, G. P. Zhang, and W. Hübner, *Phys. Rev. Lett.* **103**, 217401 (2009).
- [13] G. P. Zhang, Y. H. Bai, and T. F. George, *Phys. Rev. B* **80**, 214415 (2009).
- [14] G. P. Zhang, M. S. Si and T. F. George, *Europhys. Lett.* **94**, 17005 (2011).
- [15] M. Krauß, T. Roth, S. Alebrand, D. Steil, M. Cinchetti, M. Aeschlimann, and H. C. Schneider, *Phys. Rev. B* **80**, 180407(R) (2009).
- [16] C. S. Wang and J. Callaway, *Phys. Rev. B* **9**, 4897 (1974).
- [17] J. Bünnemann, F. Gebhard, T. Ohm, S. Weiser, and W. Weber, *Phys. Rev. Lett.* **101**, 236404 (2008).
- [18] T. Hartenstein, G. Lefkidis, W. Hübner, G. P. Zhang, and Y. Bai, *J. Appl. Phys.* **105**, 07D305 (2009); G. P. Zhang, Y. Bai, W. Hübner, G. Lefkidis, and T. F. George, *J. Appl. Phys.* **103**, 07B113 (2008).
- [19] M. S. Si and G. P. Zhang, *J. Phys.: Condens. Matter* **22**, 076005 (2010).

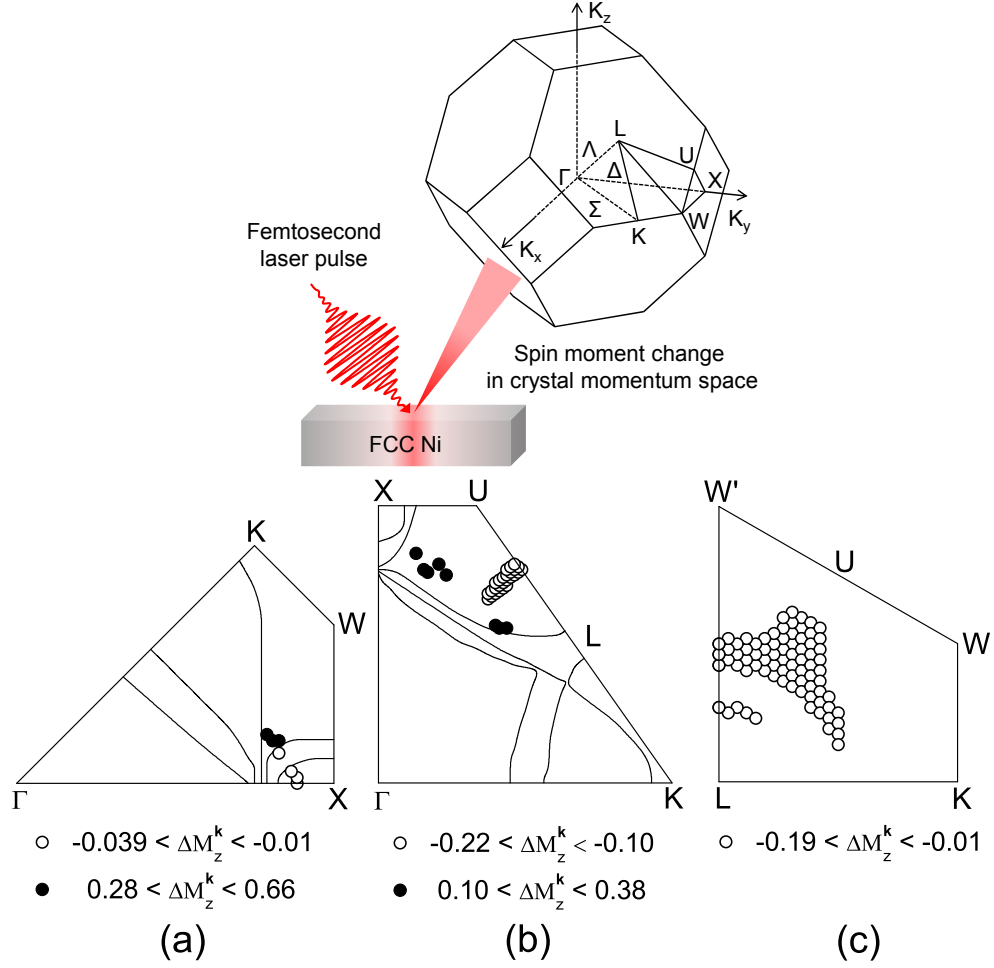


FIG. 1: Top: Femtosecond laser induced spin moment change ΔM_z^k is dispersed in the full Brillouin zone in fcc Ni. Bottom: (a) Spin moment increase (filled circles) and decrease (empty circles) in the Γ -X-W-K plane. The range of spin moment change is below each figure and in the units of μ_B . The curves denotes the Fermi surface. (b) Spin moment change in the Γ -K-L-U-X plane. There are more k points with spin moment reduction than those with moment increase. (c) Spin moment reduction dominates the hexagonal L-K-W-U-W' plane. The Fermi surface does not cross through this plane.

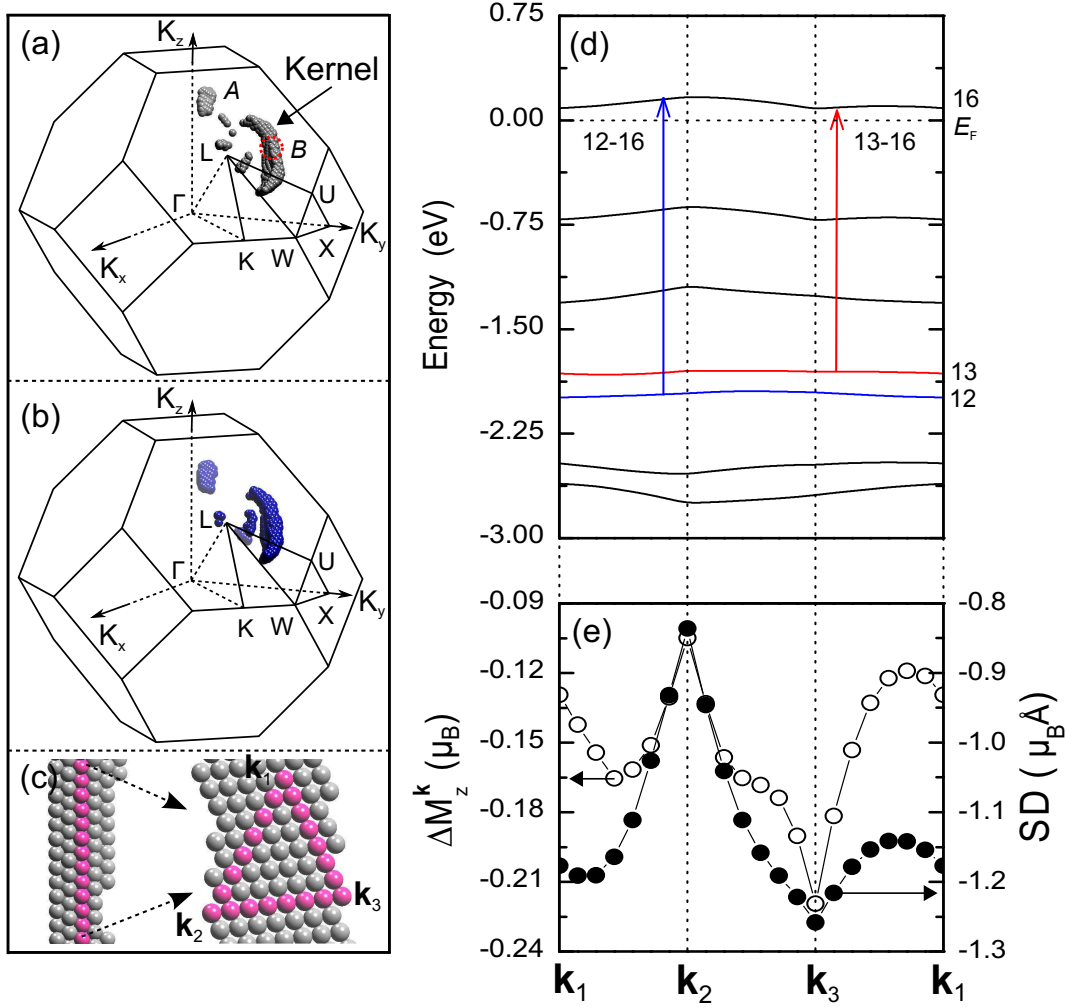


FIG. 2: (color online) (a) Hot spin spots in the three dimensional Brillouin zone. Only k points with spin moment reduction smaller than $-0.1\mu_B$ (more negative) are shown. Two hot spots are labeled by A and B . (b) Hot spin spots constructed from the maximum optical spin generator SD reduction smaller than $-0.13\mu_B\text{\AA}$. The number of these k points is the same as in (a). (c) Left: A side-view of spot B , where a stack of layers are visible. Right: One layer from spot B viewed along the plane normal. The triangle is defined by three \mathbf{k}_1 , \mathbf{k}_2 , and \mathbf{k}_3 points, with their respective coordinates of $(27, 73, 49)/104$, $(27, 73, 35)/104$, and $(34, 80, 42)/104$, in the units of $2\pi/a$. (d) Band energy dispersion of the triangle. The Fermi energy E_F is set to zero. Two dominant transitions are from level $12 \rightarrow 16$ (blue arrow) and level $13 \rightarrow 16$ (red arrow). (e) Dispersion of the optical spin generator SD (filled circles) and the spin moment change (empty circles) with crystal momentum for the triangle. The maximum reduction k points are along the \mathbf{k}_1 - \mathbf{k}_3 edge.